Earth and Planetary Science Letters 577 (2022) 117258

Contents lists available at ScienceDirect

Earth and Planetary Science Letters

www.elsevier.com/locate/epsl

Northward migration of the Javanese volcanic arc along thrust faults

Matteo Lupi [a,*], Pasquale De Gori [b], Luisa Valoroso [b], Paola Baccheschi [b], Riccardo Minetto [c], Adriano Mazzini [d]

[a] Department of Earth Sciences, University of Geneva, Geneva, Switzerland
[b] Instituto Nazionale di Geofisica e Vulcanologia, Roma, Italy
[c] Univ. Grenoble Alpes, Univ. Savoie Mont Blanc, CNRS, IRD, Univ. Gustave Eiffel, ISTerre, 38000 Grenoble, France
[d] Centre for Earth Evolution and Dynamics, University of Oslo, Oslo, Norway

ARTICLE INFO

Article history:
Received 3 April 2021
Received in revised form 28 September 2021
Accepted 21 October 2021
Available online 11 November 2021
Editor: J.-P. Avouac

Keywords:
tectonics
volcanic arc migration
Lumpur Sidoarjo - Lusi
local earthquake tomography
back-arc volcanism
Kendeng basin

ABSTRACT

East Java is characterised by a complex interaction of volcanic and tectonic processes and it is marked by isolated eruptive centres scattered across the back-arc sedimentary basins. In 2006 a large sediment hosted geothermal system named Lusi, pierced the Kendeng basin in East Java and since then it continues in a relentless eruption of mud breccia. To investigate the spatial and structural relationships between the volcanic arc and the back-arc domains, we perform a local earthquake tomography. The inversion of regional earthquakes recorded by our seismic network (for about two years) shows sharp V_p and V_p/V_s transitions. We observe a marked reduction of P-wave velocities and a high V_p/V_s ratio in the back-arc basins. Our study highlights a clear connection between the plumbing system of the volcanic arc and the northern sedimentary province. We propose a conceptual model suggesting that magmas and hydrothermal fluids may migrate from the middle to the upper crust into the sedimentary basins capitalising on existing thrust faults. Such low angle faults, promoted by the compressional regime of the region, link the magmatic domain to the northern sedimentary provinces. This process may represent the early phase of volcanic arc migration when magma-derived fluids are focused into fractured and permeable geological structures. Our conceptual model would not only help to understand the occurrence of the abundant mantle-derived fluids sampled across the back-arc, but it is also consistent with the occurrence of isolated magmatic and hybrid systems piercing across sedimentary environments in the back-arc of Java.

1. Introduction

The crustal structure of North-East Java has been the focus of great interest over the last decades due to the hydrocarbon reserves stored in the back-arc basins. The available seismic and gravimetric data provide insights about the main geological structures of the region as well as their evolution (e.g. Setiadi et al. (2019)). Several studies shed light on the ongoing crustal deformation of the Sunda arc and the structural relationships between sedimentary basins, volcanic systems and large-scale tectonics. Continuous geodetic measurements highlight strain partitioning due to the convergence of the subducing Australian plate beneath the Sunda plate (Koulali et al., 2017; Gunawan and Widiyantoro, 2019; Widjajanti et al., 2020). GPS vectors rapidly change direction rotating from East to North-East at about 111°E (Gunawan and Widiyantoro, 2019) indicating a marked discontinuity. This shift is consistent with a regional trend of NE-striking regional structures (also mapped offshore, cf. Subroto et al. (2007)) offsetting Central and East Java (Darman, 2000). Although gravimetric data (Fig. 1) show a clear separation between the volcanic arc and the sedimentary basins the North (Waltham et al., 2008) geological observations suggest that such domains are well-connected.

The interaction between the volcanic and sedimentary domains is manifested at the surface in East Java where the young sediment-hosted geothermal system (nicknamed Lusi-Lumpur Sidoarjo) initiated its activity on the 26th of May 2006. This attracted the scientific community that closely investigated East Java to study this eruption site. Lusi pierced the Earth' surface nearby a drilling site following the M6.3 Yogyakarta earthquake that occurred about 250 km distant (Elnashai et al., 2007). These spatial and temporal coincidences sparkled an active debate about whether the drilling or the earthquake activated Lusi. While the drilling argument suggests that 250 km distance falls outside one

* Corresponding author.
E-mail address: matteo.lupi@unige.ch (M. Lupi).

https://doi.org/10.1016/j.epsl.2021.117258

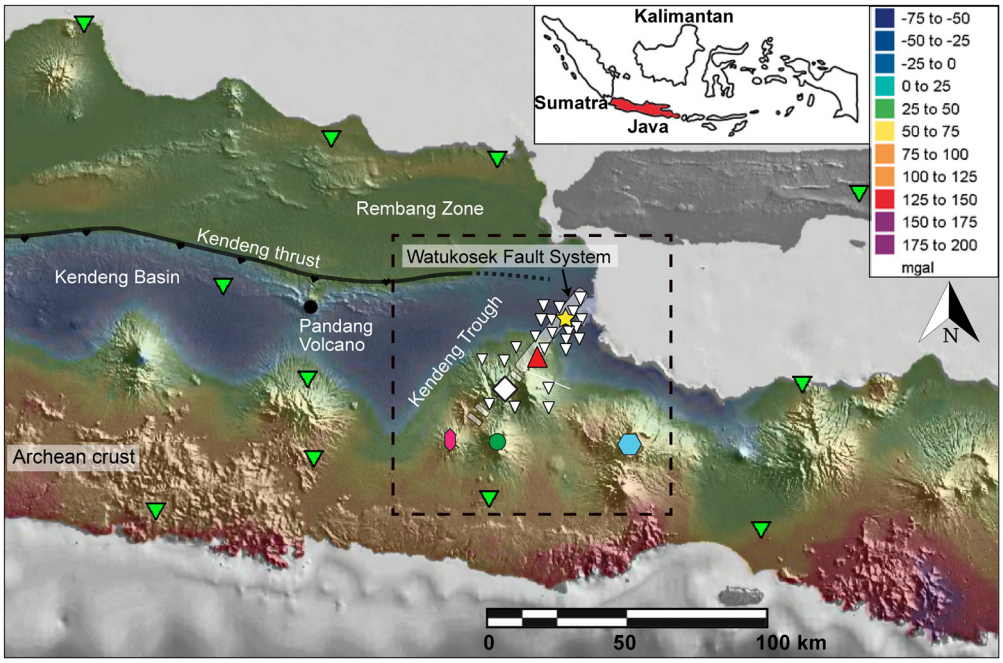

Fig. 1. Tectonic setting overlaid on Bouguer anomaly and topography. The inverted triangles show the location of the network used to compute our local earthquake tomography. In green the permanent stations from the Indonesian seismic network (BMKG). The white triangles show the LusiLab temporary seismic network. Several placemarks serve as reference throughout the figures of the manuscript: yellow star - Lusi; red triangle - Pennangungang volcano; white diamond - Arjuno-Welirang volcano; pink elongated hexagon - Kelud volcano; green circle - Kawi volcano, blue hexagon Bromo volcano (also known as Tengger caldera). The Bouguer map is taken from Smyth et al. (2005). Note that we used three additional stations of BMKG that are not shown in the map (ABJI lat: 114.23, long: -7.79; BYJI lat: 114.35, long: -8.21; RTBI lat: 114.94, long: -88.45). The black and red lines show the traces of the Kendeng thrust and suggested lineaments, respectively. The modern volcanic arc is shown by the topographic highs at the North of the ancient volcanic arc. The black dashed square frames the region investigated in this study and shown in Figs. 5 and 9. (For interpretation of the colours in the figure(s), the reader is referred to the web version of this article.)

of the empirically determined thresholds for earthquake triggering (Manga et al., 2009), the natural trigger hypothesis is supported by multiple evidences (references therein). The drilling hypothesis has been rejected by some authors not only because surface waves can trigger geological processes thousands of km away (e.g. Prejean et al. (2004)) but because the effects of the Yogyakarta earthquake were far-reaching (Harris and Ripepe, 2007). The projection of seismic waves reached the far-field perturbing Mt Merapi and Mt Semeru, about 50 and 300 km from the epicentre, respectively (Harris and Ripepe, 2007) and numerical models indicate that Lusi may have been affected too (Lupi et al., 2013).

Java's lithospheric structure has been investigated with several experiments. Wagner et al. (2007) and Koulakov et al. (2007) performed a joint inversion of passive and active seismic data and a local earthquake tomography, respectively, showing the deep plumbing systems feeding the volcanic arc of Central Java. Later, Haberland et al. (2014) have shown the accretionary nature of East and Central Java using local earthquake tomographic methods. Wölbern and Rümpker (2016) used the receiver function method to investigate the thickness of the crust beneath Central and East Java. More recently, Karyono et al. (2020) used a similar approach to further investigate the velocity structure of the Arjuno-Welirang volcanic complex in East Java.

Few ambient noise tomographic inversions helped understanding the tectonic structure of East Java. Martha et al. (2017) used seismic stations deployed from 110°E to 114°E to retrieve the shear wave velocity distributions in the upper crust of the Sunda plate (down to about 12 km depth). Focusing on the North-East part of the island, Fallahi et al. (2017) performed an ambient noise tomographic inversion revealing how magmatic bodies capitalise on regional-scale fault structures (i.e. the Watukosek fault system, Moscariello et al. (2018)) to reach and intrude the back-arc sedimentary basin (Fig. 1). The study of Fallahi et al. (2017) confirmed the geochemical data (Inguaggiato et al., 2018; Sciarra et al., 2018; Mazzini et al., 2012; Mazzini, 2018) indicating that Lusi is fuelled by magmatic and hydrothermal fluids departing from the nearby volcanic arc and migrating into the Kendeng basin (Fig. 1). A wealth of data spanning from geochemical (Sciarra et al., 2018; Mazzini, 2018; Inguaggiato et al., 2018), geological (Moscariello et al., 2018; Malvoisin et al., 2018; Samankassou et al., 2018), and geophysical (Fallahi et al., 2017; Mauri et al., 2018) observations indicate that Lusi is a natural occurrence that evolved over geological times. The large Lusi eruption provides the unprecedented opportunity to observe the evolution of a new-born hybrid system combining geochemical monitoring with regional geophysical data. To date it is still not clear how the deeper plumbing system of Lusi spatially relates (or not) with the crustal-scale magmatic system feeding the volcanic arc. However, Fallahi et al. (2017) have shown that beneath Lusi a large negative shear wave anomaly occurs. Such a marked variation was interpreted as being due to the migration of magmatic and hydrothermal fluids from the volcanic arc. It is proposed that this well-developed hydrothermal system feeds the clastic-geysering activity of Lusi (Fallahi et al., 2017). This model invoking deep magmatic bodies for the understanding of the geological processes taking place at Lusi is in line with the mantle-derived geochemical signatures of the fluids sampled in the whole region by multiple authors (Mazzini et al., 2007, 2012; Sciarra et al., 2018; Mazzini, 2018; Inguaggiato et al., 2018; Zaputlyaeva et al., 2020).

Shedding light on the spatial relationship between magmatism and hydrothermal activity in back-arc basins is particularly relevant for the understanding of the geological evolution of compressional margins. For East Java, it was suggested that Cenozoic magmatism drives the generation of hydrocarbons in the southernmost part of the Kendeng basin (Zaputlyaeva et al., 2019, 2020). Further insights on the crustal structure of the region have been brought

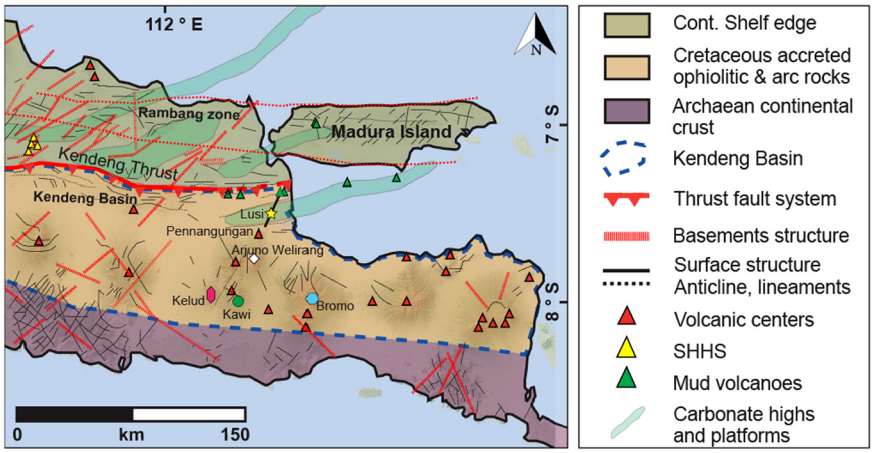

Fig. 2. Simplified geological and tectonic map of East Java. The red triangles show the position of volcanic systems, yellow triangles indicate the location of sediment hosted geothermal systems and green triangles show the location of mud volcanoes. The main tectonic features are also shown along with the main lithostratigraphic units. Compiled from (Clements et al., 2009; Istadi et al., 2009; Sribudiyani et al., 2003; Smyth et al., 2005; Moscariello et al., 2018; Novianto et al., 2020).

forward by Karyono et al. (2020). However, we argue that inaccuracies occur in the seismic catalogue used by Karyono et al. (2020). Hence, interpretations of crustal structures derived from Karyono et al. (2020) shall be handled with care and revised. This aspect is discussed in detail in the supplemental material.

Mazzini et al. (2012) proposed that the birth of Lusi could represent the early manifestation of the northwards migration of the volcanic arc. Certainly, the geochemical, geological and geophysical experiments mentioned above point out a complex tectonic setting marked by well-developed deep-reaching geological structures and well-marked mantle-derived/driven processes. Geological observations from other localities in the Java island also reveal the presence of active systems in the Kendeng basin releasing mantle-derived fluids (Mazzini et al., 2014). These observations substantiate a progressive migration of magmatic fluids in the back-arc of the island. The exact mechanisms and pathways through which the northwards evolution of the volcanic arc occurs remain to date poorly constrained. The local earthquake tomography that we present in this work helps understanding the large-scale crustal structure and the spatial relationship between the volcanic arc and the back-arc basin in East Java.

The manuscript is structured as follows. First, we introduce the geological setting of the investigated region followed by the description of the seismic experiment and the seismic catalogue. Next, we show the results (the resolution tests are shown in the supplemental online material). We then discuss our findings and conclude with observations that may be relevant to promote an updated tectonic model of the region.

2. Geological setting

Fig. 2 shows the key tectonic features and the geological domains of East Java. The Bouguer anomaly (Waltham et al., 2008) that we overlay on the digital elevation model in Fig. 1 depicts at least three clear domains. In the South crops out the volcanic arc that was active during the Eocene to Early Miocene. The high Bouguer anomalies of the ancient volcanic arc are reduced to about 25-50 mgal beneath the currently active volcanic arc. The transition to the sedimentary environment of the Kendeng basin is sharp. Here the Bouguer anomaly drops to negative values (down to about -75 mgal) with the lowest values found in the depocentres of the basins.

The structural limits of the geological domains constituting Central and East Java are sealed by well-developed tectonic structures (Fig. 2). The Kendeng basin is pierced by active volcanic systems such as the Pandang and the Pennangungang Volcanoes (Fig. 1). The recent seismic crisis occurred in 2016 nearby Mount Pandang highlighted the possible presence of magma in the shallow crust of this region (Santoso et al., 2018). Similar observations were drawn by Fallahi et al. (2017) who showed the occurrence of a well-defined magmatic reservoir below the Pennangungang volcano, that is a Quaternary system interrupting the lateral continuity of the Kendeng basin. Further North, the Kendeng basin is sealed with the Rembang zone by the Kendeng thrust. The back-arc features a well-developed fold and thrust belt (Novianto et al., 2020) and the whole East Java is affected by NE-striking regional lineaments. These are interpreted by Subroto et al. (2007) as the prolongation of the large-scale en-echelon structures highlighted by Darman (2000) in the Java Sea. Fallahi et al. (2017) highlighted the importance of one of such NE-striking faults (i.e. the Watukosek fault system) in connecting Lusi with the volcanic arc. Mazzini et al. (2012) and Lupi et al. (2018) proposed that the observed transition from magmatic to sedimentary volcanism in East Java would follow a NE-striking direction becoming visible along the Watukosek fault system upon which Lusi developed. Along this NE-striking directions crop out eruptive structures emitting fluids with mantle signatures (Zaputlyaeva et al., 2019). This could be explained by the occurrence of magma at shallow depth (Zaputlyaeva et al., 2020) that would in turn accelerate hydrocarbon maturation, development of elevated pore pressures and ultimately eruptive hydrothermal activity such as the one found today at Lusi. Indeed, the East Java basin hosts the widespread presence of diapiric structures that pierce the sedimentary deposits. The seismic profiles shown by Mazzini et al. (2007), Mazzini et al. (2012) and Moscariello et al. (2018) highlight seismic reflectors deflected upwards possibly deformed by elevated pore pressures. It has been proposed that such gravitative processes may have led in the past to the formation of systems similar to Lusi. For instance, the well of Porong (Istadi et al., 2009) pierces through seismic reflectors titled downwards. Mazzini et al. (2012) suggested that the morphology of such reflectors may be due to the deflation of a paleo-piercement erupting in the past at the site of Porong.

3. Seismic network and data

We used the temporary seismic network deployed around the Arjuno Welirang volcanic complex, the Watukosek Fault System, and the Lusi eruption site in the framework of the LusiLab project

Table 1
Number of picks for each phase and weight of the picks.

Total number of events = 588		
Readings P-Waves	9540	
....weight 0	2179	(22.84%)
....weight 1	3253	(34.09%)
....weight 2	2617	(27.49%)
....weight 3	1491	(15.62%)
....weight 4	0	0%)
....weight 9	0	0%)
Readings S-Waves	7047	
....weight 0	825	(11.70%)
....weight 1	2268	(32.18%)
....weight 2	2770	(39.30%)
....weight 3	1176	(16.68%)
....weight 4	8	(0.11%)

(Mazzini, 2018) (white triangles in Fig. 1). We refrain from describing the distribution of the stations since it was previously introduced by Fallahi et al. (2017), Obermann et al. (2018), and ultimately by Karyono et al. (2020). We manually re-picked all the events of the seismic catalogue of Karyono et al. (2020), significantly increasing the number of P- and S-wave arrival times. We found shortcomings in the catalogue of Karyono et al. (2020) due to the lack of picking of S-waves (see supplemental online material). The lack of S-wave pickings may have led Karyono et al. (2020) to biased tomographic results (see supplemental material). To increase the number of S-wave pickings, we integrated the LusiLab network with the permanent stations of the Indonesian seismic network (BMKG) (Fig. 1 and S1) improving the localizations of the seismic events used for the local earthquake tomography (Figure S2 in the supplemental online material).

After integrating the LusiLab network, we scanned the continuous 3-component waveforms of each seismic station looking for seismic events. We used two different earthquake detection algorithms. First, we ran an STA/LTA routine that detected 595 events. Then, we further scanned the seismic records with *LASSIE*, a coherence-based detector working particularly efficiently in noisy environments for the detection of microseismicity (Comino et al., 2017; Antunes et al., 2020). This second step allowed us to obtain 41 additional events. Next, we picked all the available P- and S-wave arrivals using non-filtered data (and/or filtered waveforms on noisy data) in Hypoellipse (Lahr, 1999) using vertical and horizontal components. The manual picking procedure allowed us to collect 9540 P-wave arrivals and 7047 S-wave arrivals. The weights of the phases are shown in Table 1.

Out of the 636 identified events, we discarded 48 earthquakes and retained 588 events. Following the weighting scheme proposed by Lahr (1999), we inverted P- and S-wave arrival times with Hypoellipse (Lahr, 1999) using the 1D velocity model of Obermann et al. (2018) and using a V_p/V_s ratio of 1.77 to localise the earthquakes. We also tested additional velocity models (Haberland et al., 2014; Koulakov et al., 2007) finding no remarkable difference for our scope. Fig. 3 shows the seismic events recorded in our catalogue. Most earthquakes are located off-shore (South of) Java at hypocentral depths ranging from 30 to 70 km. The hypocentre distributions suggest that they are related to the subduction of the Indo-Australian plate. These events are characterised by large-amplitude S-waves recorded about 20-25 seconds after the P-waves. At recording sites located on the southern sector of the island, P- and S-wave arrivals are separated by about 10-15 seconds.

Since subduction earthquakes represent the majority of the recorded seismicity, our study area is not affected by a marked seismic activity, contrary to what suggested by Karyono et al.

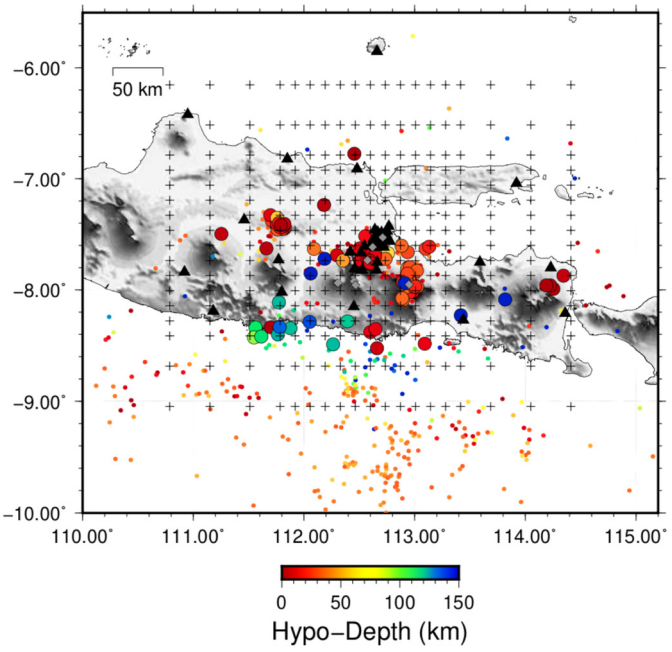

Fig. 3. Location of the earthquakes used to perform the tomographic inversion. Only the events falling inside the network and satisfying certain selection criteria (i.e. recorded by at least 6 stations and with location error smaller than 10 km and RMS within 1.5 s) were used to perform the tomographic inversion. This restrained the whole catalogue to 128 seismic events shown by the larger circles falling inside our network. Our catalogue counted 1892 P- and 1468 S-wave arrival times.

(2020). However, by adding further stations of the national network located to the South (Figure S1), it was possible to widen the target area including some seismogenic volumes located East and West of Lusi and surrounding zones. These additional data allowed us to sample the crustal volume below the volcanic region South of Lusi. Finally, to perform the travel time tomography, we selected only the events falling inside the network (identified by larger circles in Fig. 3) and recorded by at least 6 stations and with location error smaller than 10 km and RMS within 1.5 s. These selection criteria are satisfied by 128 events providing a total of 1892 P- and 1468 S-wave arrival times. These have been used as input for our travel-time tomography. In Figure S4 of the supplemental material, we show histograms reporting the frequency distribution for number of phases, location errors, RMS and azimuthal gap of the selected events. The dense crossing of seismic rays inside the target volume is a crucial aspect to obtain stable and robust tomographic models. We acknowledge that the number of available events (128) does not represent a populated dataset if compared to recent tomographic models of other volcanic regions (e.g. Koulakov et al. (2007)). However, the use of accurate P- and S-waves arrival times ensures that recovered anomalies are a reliable expression of the first order crustal features of the region.

4. Methods

We used the *Simulps14* code to obtain 3D V_p and V_p/V_s models of the region framed in Fig. 1 (Eberhart-Phillips and Reyners (1997) and references therein). The inversion code allows a simultaneous inversion for the source location as well as the subsurface V_p and V_p/V_s structure using an iterative and damped least-square approach. The tomographic model is parameterised by a three-dimensional regular grid of nodes with velocity continuously defined through the medium following trilinear interpolation functions. For each node, the initial V_p and V_p/V_s (= 1.77) are taken from the 1-D V_p model of Obermann et al. (2018) and from the result of the Wadati regression, respectively. We chose a grid of

nodes spaced 15 km horizontally and 5 km in vertical direction (Fig. 3) as the best compromise between misfit reduction and spatial resolution of anomalies (see the supplemental online material for the resolution tests). We set the damping values of 200 and 400 for V_p and V_p/V_s models, respectively, based on the analysis of the trade-off curves. After two iteration steps, we obtained a final RMS of 0.55 s corresponding to a variance improvement equal to 39%.

We investigated the accuracy of our tomographic model by analysing the full resolution matrix (Menke, 1984) and performing a restoring test (Zhao et al., 1992). The resolution matrix is a symmetric matrix, computed in the frame of a damped least square inversion, where each column represents the averaging vector of a generic parameter. Its diagonal elements indicate the resolution of a given node while the off-diagonal elements quantify how nearby nodes contribute to the computation of that parameter. A well-resolved node is characterized by an averaging vector picked around a diagonal element close to 1, with small off-diagonal elements (Menke, 1984). We use the Spread Function (SF, Michelini and McEvilly (1991)) that quantifies how an averaging vector is picked around its diagonal value by weighting the off-diagonal contributions with the geometrical distance from the observed node. Small values of SF indicate good compact averaging vectors and thus good resolution. Large values of SF indicate poorly resolved nodes due to the strong contributions of off-diagonal nodes. The best way to identify a reliable threshold for well-resolved parameters is to report, in a two dimensional plot and for each node, the SF and the ray density expressed by the derivative weight sum (DWS, following Toomey and Foulger (1989)). The distribution of the SF and DWS values usually defines a L-shaped trend, with DWS decreasing as SF gradually increases, since the resolution is strongly dependent on the amount of data constraining the velocity in each node. The kink of the L-shaped trend corresponds to the upper threshold of SF that ensures a well-resolved node and negligible smearing effects (Toomey and Foulger, 1989). Based on the observed SF versus DWS distribution (see Figure S3 of supplemental material), we set the SF threshold to 3.0. We further check the reliability of the observed tomographic features performing a restore resolution test (Zhao et al., 1992). The final V_p and V_p/V_s models are used as synthetic model where the forward problem is used to compute synthetic travel-times using the same source-receiver distribution of the real datasets. To simulate the real dataset, Gaussian white-noise with standard deviation deduced from the real inversion (0.49 s and 0.55 s for P- and S-wave data, respectively), has been added to synthetic travel-times. The new travel times have been re-weighted according to the new noise level. We then inverted the final dataset using the same starting model (Obermann et al., 2018) and the same inversion parameters used in the real case. Results of the test are shown in the supplemental material (Figure S8) for the layers at 0 and 5 km depths. We show the final models computing the percent deviation (%) from the starting velocity model. Synthetic tests show that, inside the well resolved part of the models (SF<3), the deviation of the final models from the input model is within 5% for both V_p and V_p/V_s. Thus, results of synthetic tests and the analysis of the resolution matrix indicate that V_p and V_p/V_s models are reliable within the volume with SF $\leq$ 3.0. To visualize the spatial definition of averaging vectors, we plotted the 70% smearing contour for nodes with a spread function lower than or equal to 3.0 (see Figures S5 and S6 of Supplementary material), thus respecting the criterion of Toomey and Foulger (1989) (see also Eberhart-Phillips and Chadwick (2002)).

The best resolved region (i.e. where the SF is $\leq$ 3.0 and narrow smearing effects) occurs in the centre of the network. It is centred around the Kelud-Arjuno-Welirang-Lusi volcanic district (see supplemental online material Figures S5 and S6). Further away from this volcanic district and towards greater depths, the smearing effect increases but it is confined to the adjacent nodes. The smearing is more evident for V_p and V_p/V_s models at 10 km depth between the two volcanic complexes, due to the decreasing of earthquakes and thus of the ray coverage.

5. Results of the local earthquake tomography

The 3D velocity models are shown first as absolute values (Fig. 4) and then as percent differences with respect to the 1D starting model. Horizontal slices of the inverted results at different depths are shown in Fig. 5. Fig. 6 shows the directions of the vertical cross sections reported in Figs. 7 and 8. The absolute V_p and V_s velocities indicate a drop in the northeastern region, i.e. in the Kendeng basin below Lusi. At greater depth, such lateral variations are still marked in the distribution of the V_s (i.e. at 5 km depth) and V_p (i.e. at 10 km and 15 km depth). Values of V_p/V_s particularly high (i.e. about 1.82 at 5 km depth) are driven by low V_s. Shallow low V_p velocities follow the geological limits of the Kendeng basin. Overall, the results indicate heterogeneities in V_p and V_p/V_s, with sharp velocity contrasts. At shallow depths (e.g. 0 and 5 km depth), Fig. 5 shows that the region is split into three domains characterised by V_p perturbations from South-West to North-East of about -5%, 15% and -15%. Such sharp transition is also found in the V_p/V_s where anomalies of each domain are about 2%, -4%, and 4%.

The shallow crust immediately below the volcanic arc features positive (i.e. about 15%) and negative (i.e. -5%) V_p and V_p/V_s anomalies, respectively (Fig. 5). While until 5 km depth, the shape of the lobes of V_p and V_p/V_s perturbations broadly corresponds to one another. At about 10 km depth the shape of both the V_p and V_p/V_s anomalies becomes dissimilar. The central positive V_p anomaly (e.g. at 0 km and 5 km depth) is SE-striking while the V_p/V_s negative anomaly is elongated towards the North. Within the upper 5 km, the central high V_p anomaly corresponds to a negative V_p/V_s anomaly. At 10 km depth, we no longer recognise a positive central V_p anomaly and the three distinct domains of V_p anomalies are no longer visible. Lusi sits at about the centre of the negative V_p anomaly (about -5%) and where the V_p/V_s anomaly is positive. At 15 km depth the inversion holds similar results with anomalies more pronounced. Deeper than 15 km depth, the anomalies become less pronounced and we find no more negative V_p/V_s anomalies in the central region. Instead, a positive V_p/V_s anomaly is recognised below Lusi (that is no longer visible at 20 km depth) and below the volcanic arc. The region comprised between the Bromo caldera, the Arjuno-Welirang volcanic complex and the Butak volcano features positive V_p/V_s anomalies deeper than 15 km depth.

The cross sections striking N45 (Fig. 7) consistently show a high V_p anomaly progressively moving northwards across the vertical slices. The corresponding V_p/V_s anomaly shows positive values around 3%. The central high V_p anomaly is neighboured by prominent V_p negative anomalies that are sub-horizontal in the South-West at about 20 km depth and progressively steepen towards the North-East, i.e. in the Kendeng region. In the central part of the volcanic arc (Fig. 7C-C') the low V_p anomaly fully embeds the central positive V_p anomaly. V_p/V_s ratios in this region are as high as 5%. The cross sections striking N135 (Fig. 8) show that at about 15 km depth occurs a sub-horizontal discontinuity separating high and low V_p anomalies. The shallow crust shows V_p velocities higher than the ones of the 1D velocity model derived for the region. Vice-versa, the lower crust features negative V_p anomalies. The easternmost profile (Fig. 8H-H') shows marked negative V_p anomalies and positive V_p/V_s anomalies beneath Lusi. The most prominent values of negative V_p/V_s occur at about 5 km depth.

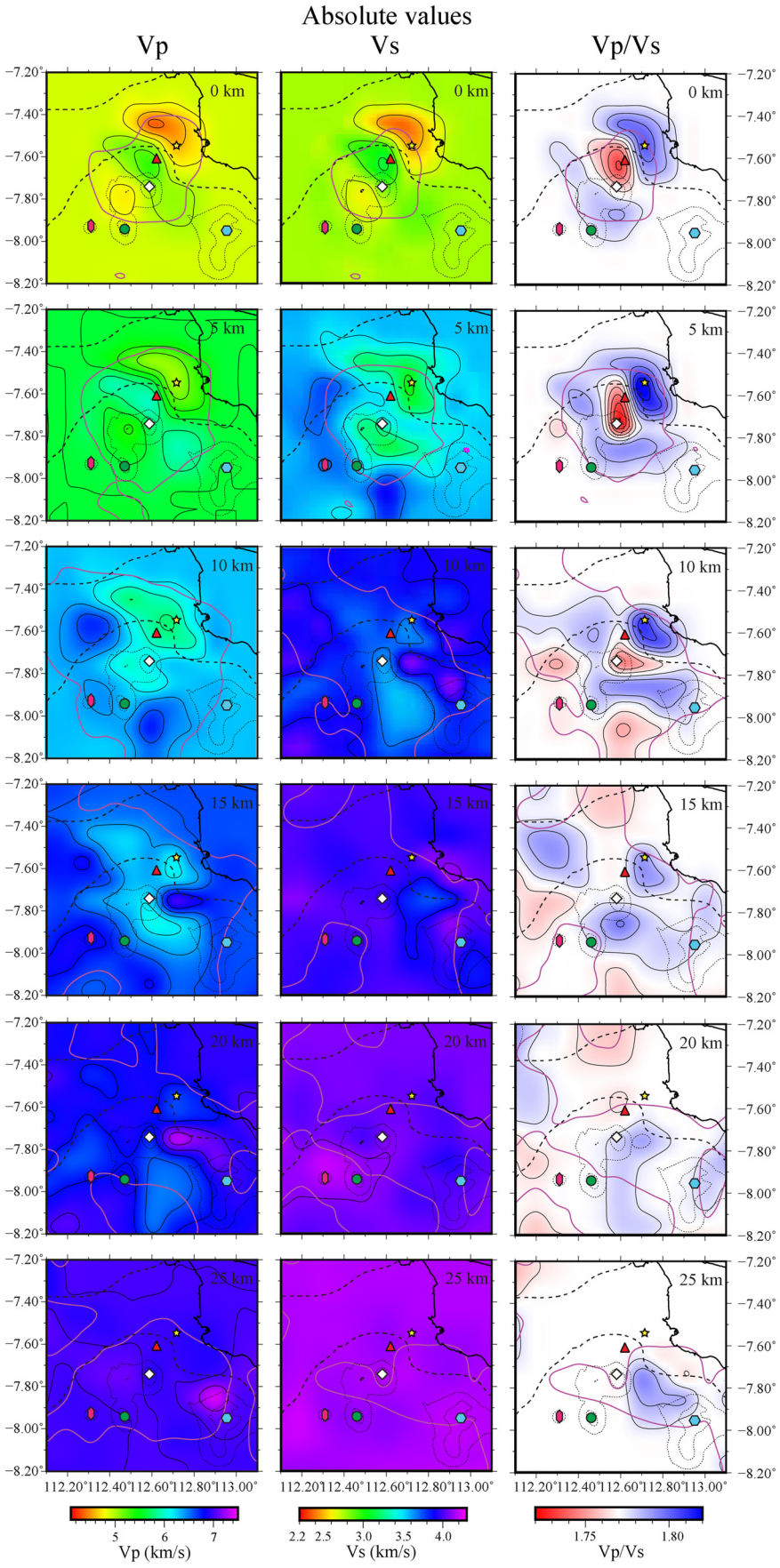

Fig. 4. Inverted V_p, V_s and V_p/V_s values. At shallow depths the spatial variations of V_p and V_s are prominent and drive the high V_p/V_s ratio found in the back-arc (i.e. in the Kendeng basin below Lusi). V_p and V_s variations become smoother at greater depths. The dashed line shows the main limits of the Bouguer anomaly of Smyth et al. (2005) shown in Figs. 1 and 9. For the place-marks refer to the caption of Fig. 1.

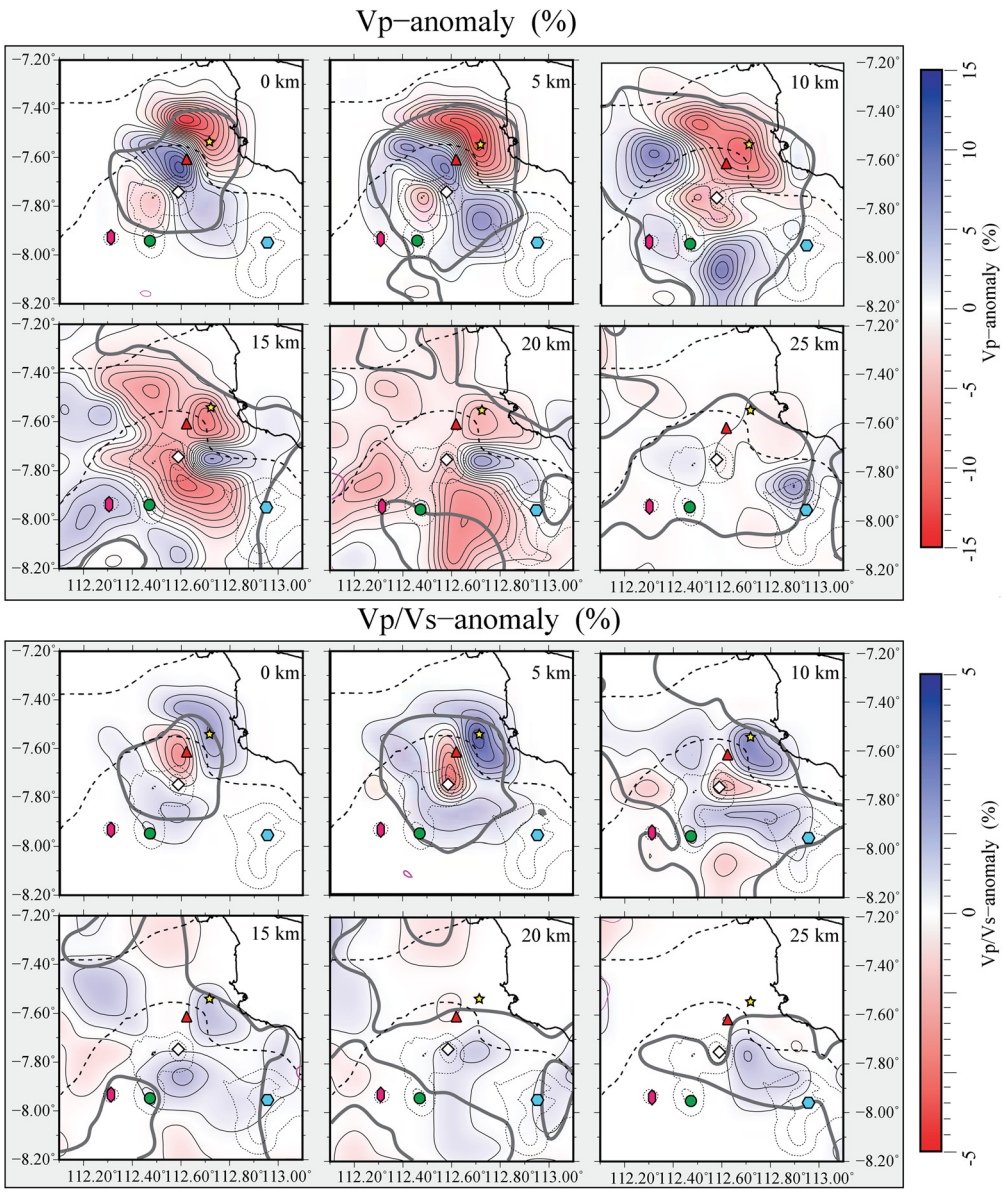

Fig. 5. Inverted V_p and V_p/V_s anomalies. At shallow depths the northern and southern negative V_p anomalies are separated by a positive V_p anomaly region. At 10 km depth the back-arc is connected to the arc by a domain characterised by negative V_p anomalies. The distribution of high V_p/V_s anomalies is separated by a region of low V_p/V_s anomalies up to about 10 km depth. The bold grey contours outline the confidence limits of the inversion. The dashed line shows the main limits of the Bouguer anomaly of Smyth et al. (2005) shown in Figs. 1 and 9. For the place-marks refer to the caption of Fig. 1.

6. Discussion

In order to be able to properly identify S-picks in the recordings used for the tomography, we have included the records of permanent seismic stations (even if they were outside of the study area of the tomography). This resulted into a larger network characterised by an heterogeneous spatial distribution of the seismic stations that affected the grid size. Fig. 1 shows that out of 44 seismic stations, 31 are closely distributed around Lusi (LusiLab network used also by Karyono et al. (2020), while 13 stations have a larger spacing. The finest grid that we could use in the inversion is 5 km and 15 km on the vertical and horizontal directions, respectively. It follows that we are not able to resolve local features. For instance, the shallow magma chamber beneath Pennangungan or the NE-striking conduit linking the volcanic arc to Lusi shown by Fallahi et al. (2017) cannot be resolved. Our inversion, instead focuses on large-scale crustal domains providing information on the lateral and vertical extension of major sedimentary basins, major crustal suture zones (e.g. geological lineaments and thrusts) and magma transport in the crust.

6.1. Sharp transitions between geological domains

In agreement with Wagner et al. (2007), we find that the most prominent reduction of V_p and V_s occurs in the northernmost portion of the volcanic arc and further north. Our negative anomalies are about 5% less prominent than the ones found by Wagner et al. (2007) in the volcanic arc. The V_p and V_p/V_s perturbations retrieved from our inversion of the seismic data are often sharp. We speculate that the volcanic arc is characterised by negative V_p perturbations and high V_p/V_s ratios. The resolution of our tomography does not allow us to highlight possible shallow magmatic reservoirs below the volcanic arc. Low V_p and V_p/V_s perturbations become prominent in the volcanic arc from 10 km depth downwards (Fig. 5). At shallower depths, high V_p perturbations characterise the upper crust in the arc region. The most promi-

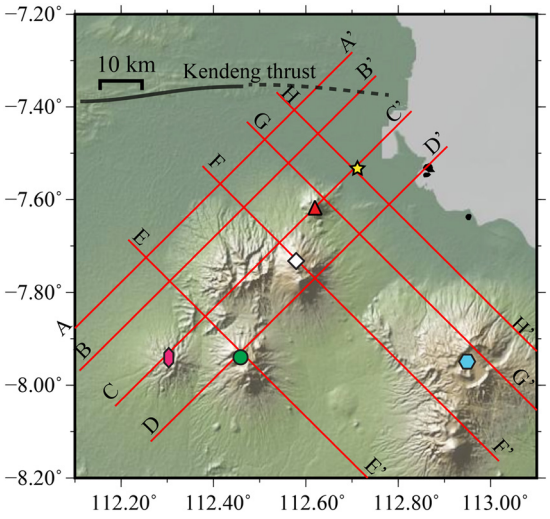

Fig. 6. Locations of the cross sections. The red lines show the positions of the vertical cross sections shown in Figs. 7 and 8. We selected the NE-striking orientation as this is the direction of the alignment of the volcanic system from Kelud to Lusi. The NW-striking sections are perpendicular to N45 profiles.

nent negative V_p and positive V_p/V_s perturbations are found in the Kendeng basin. Here, Fallahi et al. (2017) have shown an extreme reduction of shear wave velocities suggesting the occurrence of a well-developed hydrothermal system fuelled by shallow intrusions. The widespread occurrence of fluids pervading the northern region of the Kendeng basin, where Lusi resides, is also suggested by the anomalies retrieved in our study (Fig. 5). In addition, the back-arc of East Java is a region characterised by an abundant presence of hydrocarbons. This evidence, combined with the possible occurrence of magma at shallow depth and a vigorous crustal hydrothermal circulation (Fallahi et al., 2017) would support the reduction of V_p velocities and the high V_p/V_s ratios that we find in the region. Such highly reduced values are found in the region by Karyono et al. (2020) who show an almost vertical conduit reaching down to at least 20 km depth. However, Karyono et al. (2020) uses a catalogue that does not consider S-wave arrivals (*verbatim: "the onsets of S-waves are too emergent to be reliably picked for the large majority of events and are therefore not considered")*, resulting into location errors (Figure S2). For this reason, we re-assessed the seismic catalogue of LusiLab previously used by Karyono et al. (2020) to perform our local earthquake tomography presented here. We found that out of the 797 earthquakes used by Karyono et al. (2020), more than 650 earthquakes fall outside the network when using the S-wave arrivals that are well-visible on stations of the Indonesian seismic network. The vast majority of the events used by Karyono et al. (2020) is therefore mislocated by more than 100 km (Figure S2). The corollary is that the catalogue of Karyono et al. (2020) shall be revised and results reconsidered.

For the tomographic inversions we could use a low number of events (resulting into 1892 P- and 1468 S-wave arrival times). However, the resolution tests (Figure S8) show that we could resolve the velocity structure of the investigated region. The dashed line in Fig. 5 shows the outline of the Bouguer anomalies bounding the Kendeng basin presented by Smyth et al. (2005). We observe that the change between low and high V_p anomalies shown in Fig. 5 broadly corresponds to the transition between the recent volcanic arc and the back-arc basin (where the Bouguer anomaly is about 0 mgal, Fig. 1). Regional-scale gravimetric measurements are available via the *International gravimetric bureau*.[1] Fig. 9 highlights that the Kendeng basin and the volcanic arc are characterised by negative and positive Bouguer anomalies, respectively. The transition at 0 km depth between positive and negative V_p anomalies well-mimics the -30 mgal isoline shown by the gravimetric data. However, we observe no correspondence between positive Bouguer anomalies and negative shallow (i.e. between 0 and 5 km depth) V_p anomalies in the volcanic arc. The volcanic arc shows positive Bouguer anomalies suggesting the occurrence of denser bodies (e.g. possibly juveniles magmas) below the volcanic edifices. We notice that the positive Bouguer anomaly of about 100 mgal volcano corresponds to the location of a prominent negative V_p and positive V_p/V_s perturbation roofing at 10 km depth (Fig. 7D-D'). Unfortunately, we have no resolution below Bromo to investigate the marked positive Bouguer anomaly highlighted by the gravity data and confirmed by previous authors (Smyth et al., 2005; Maryanto et al., 2017).

6.2. A tectonic model for the northward progression of the volcanic arc

The NE-striking tomographic cross-sections (Fig. 7) show that the arc and the back-arc regions are connected by an almost continuous negative V_p perturbation that characterises the crustal volume spanning from 10 to 25 km depth. At shallower depth (0-5 km), this continuity is interrupted by a volume of positive V_p perturbation located beneath the Pennangungan volcano. Fig. 5 shows that this region, comprised between Welirang and Pennangungan volcanoes, is characterised by positive V_p and negative V_p/V_s. We speculate that such a high V_p anomaly may represent plutonic domains (e.g. ancient magmatic reservoirs) brought to shallow depths along low-angle thrust faults driven by an overall compressional tectonics. This mechanism has been proposed elsewhere in compressive settings to explain lower-crust and mantle units cropping out in fold and thrust belts (e.g. in the Alps Rosenberg and Berger (2009)). The low-angle thrust faults have been proposed to characterise the Kendeng basin and the back-arc of East Java (Nachrowi et al., 2003; Clements et al., 2009; Simo et al., 2012). This compressional tectonics generates well-developed broad anticlines and synclines visible in the active seismic data that prospected the Kendeng Basin (Mazzini et al., 2007, 2009; Moscariello et al., 2018; Novianto et al., 2020). The compressional and dilatational state of the upper crust is pointed out by (Gunawan and Widiyantoro, 2019) who calculate the dilatation rate of the region. Their modelled geodetic data show a well-developed compression for the northern part of East Java. However, while the back-arc is in compression (including Lusi), the region of the volcanic arc seems to be less compressed, almost in extension. The compressive tectonics characterising the setting is also supported by the widespread presence of piercement structures propagating vertically across the anticlines that deformed the upper sedimentary sequence (Mazzini et al., 2007, 2009; Moscariello et al., 2018). In the northern part of the Kendeng Basin, these structures also control the position of several piercements, some of which reach the surface creating mud volcanoes (e.g. Kalang Anyar, Gunung Anyar, Pulungan, Pangangson, Dawar Blandong). Closer to the volcanic arc, surface-breaching piercements form sediment hosted geothermal systems that are fuelled by shallow magmatic intrusions (Mazzini et al., 2012; Fallahi et al., 2017; Lupi et al., 2018). Fig. 2 shows that there is a progressive transition from magmatic to sedimentary eruptive centres aligned along a NE-striking direction. We observe that this region corresponds to the extension of the Watukosek fault (Mazzini et al., 2007; Fallahi et al., 2017). Compressional tectonics and volcanism are common occurrences in subduction settings. As proposed by Menand et al. (2010) sub-horizontal dike propagation, i.e. sill intrusion, is favoured in stratified sedimentary units of compressional settings. In this framework, the thick sedimentary cover composing the Kendeng basin is an ideal environment for the sub-horizontal spreading of sills departing from the volcanic

[1] http://bgi.omp.obs-mip.fr.

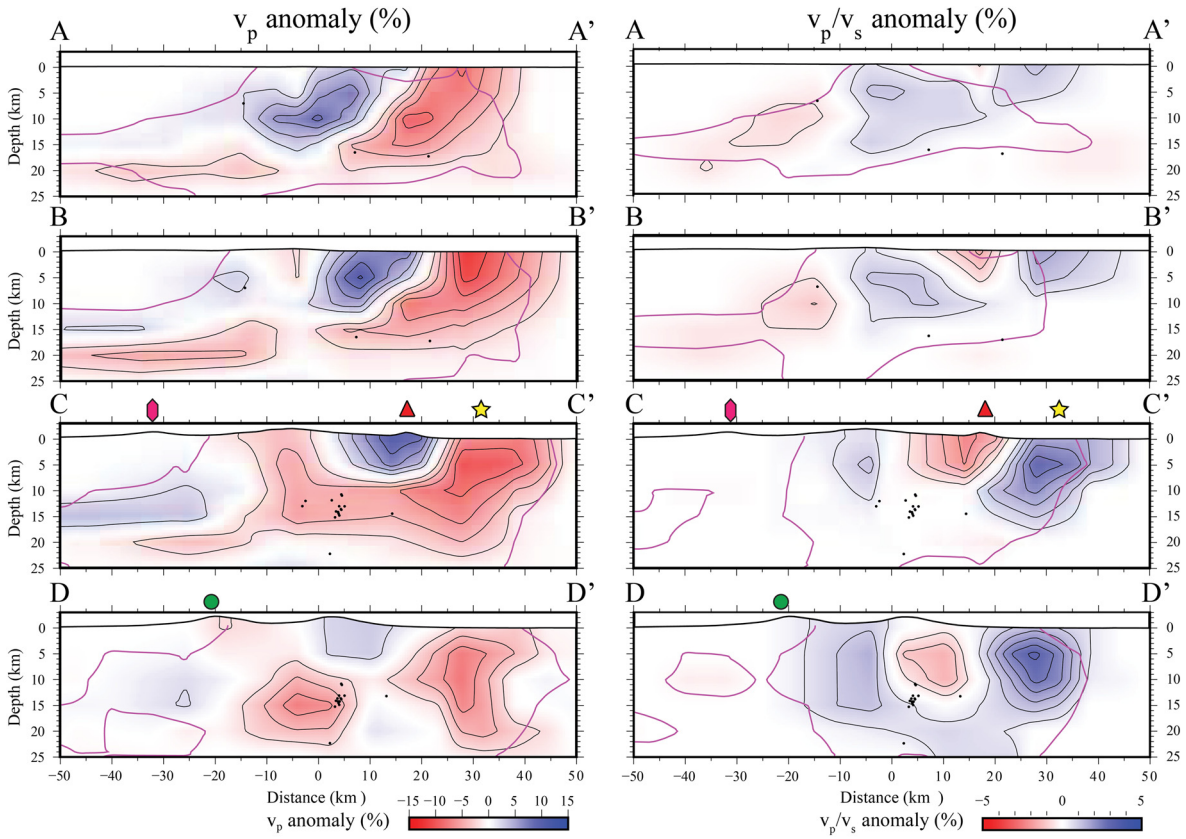

Fig. 7. Inverted V_p and V_p/V_s anomalies. A negative V_p anomaly connects the volcanic arc to the Northern sedimentary basins. Beneath Pennangungang (red triangle) we notice a positive V_p anomaly and a low V_p/V_s ratio. We propose that these may represent thrusted plutonic units brought to shallow depths along low-angle faults. The region of the volcanic arc is well-shown in section C-C' and characterised by negative V_p and positive V_p/V_s anomalies.

arc into the back-arc. For instance, Galland et al. (2007) propose that magmatic progression during crustal shortening may have fed the Tromen volcano in Argentina and the Boulder Batholith in Montana. This mechanism is also widely used to explain the emplacement of granitic bodies at shallow crustal levels. Ferré et al. (2012) shows with laboratory experiments that the occurrence of existing flats-and-ramps favours the migration of crustal melts ultimately leading to the emplacement of granitic bodies in the upper crust.

The variation of V_p and V_s velocities shown in Fig. 4 and their reduction (Figs. 5, 7, and 8) may be explained by overpressured fluids developed during the hydrocarbon maturation process within the thick sediments of the Kendeng basin without invoking the occurrence of magma. This may be in line with the eruptive activity taking place at Lusi. The low Bouguer gravity anomaly of the Kendeng Basin could also be explained by a thick sedimentary cover that would also cause low V_p velocities and high V_p/V_s ratios. However, the geochemical data show a marked mantle component in the fluids erupted at Lusi that may only be explained by the occurrence of magma at depth (Mazzini et al., 2012; Inguaggiato et al., 2018; Zaputlyaeva et al., 2019). Such geochemical signatures could not be explained by the hydrocarbon maturation process and a thick sedimentary cover alone. Because of this, we propose a new scenario that would help understanding the birth of Lusi and that would reconcile the multidisciplinary observations carried on the region over the last decade. Fig. 10 proposes a conceptual tectonic model to illustrate the structural progression of the volcanic arc in East Java. The quasi-frontal convergence of the Indo-Australian and Eurasian plates in East Java causes the formation of the volcanic arc and a well-developed compressional regime. Gunawan and Widiyantoro (2019) suggest that the compressional principal strain rate in this region is NE-striking and about 15 μstrain yr^{-1}. The shear strain rate is well-developed in the Kendeng basin, and it is the highest of the region where Lusi appeared (99 μstrain yr^{-1}, Gunawan and Widiyantoro (2019)). This results in the formation of a fold and thrust region characterised by low-angle faults departing from below the volcanic arc (Clements et al., 2009; Haberland et al., 2014). We propose that magmas capitalise on such low-angle regional-scale thrusts to migrate into the back-arc. Dikes propagate parallel to S1 (e.g. Tibaldi (2005)). In the back-arc of compressive margins where compression is particularly developed, dike to sill transition often occurs along sedimentary lithostratigraphic interfaces as shown by e.g. Menand et al. (2010) who suggest that the strong compressional regime may hinder the vertical intrusion of dikes favouring lateral progression. The occurrence of magma intruding in the back-arc may help explaining the high mantellic He concentrations sampled in the fluids erupted at Lusi while reconciling the marked drop of V_s and the high V_p/V_s ratios shown by our tomography. This also provides support for the presence of structures such as Pandang Volcano (Fig. 1) or other Lusi-like hybrid systems such as Bledug Kuwu, Bledug Cangkring Kropak, Mendikil, and Bledug Banjarsari located in the back-arc of the island further away from the investigated region. Furthermore, this also well-fits the negative V_p anomalies that seem to connect the volcanic arc with the back-arc basins (Fig. 7B-B' and C-C'). Our model is in agreement with geochemical data showing a marked mantle signature in the fluids sampled at various locations across the region (Mazzini et al., 2012; Sciarra et al., 2018; Inguaggiato et al., 2018; Zaputlyaeva et al., 2019). Such a mantle-derived signature is progressively less prominent further away from the volcanic arc, although it can still be detected at some of the mud volcanoes located close to the Kendeng thrust, near the Madura strait (Mazzini et al., 2012). Anticlines and synclines are well-mapped in the Kendeng thrust and in the Rembang zones (Hall et al., 2007;

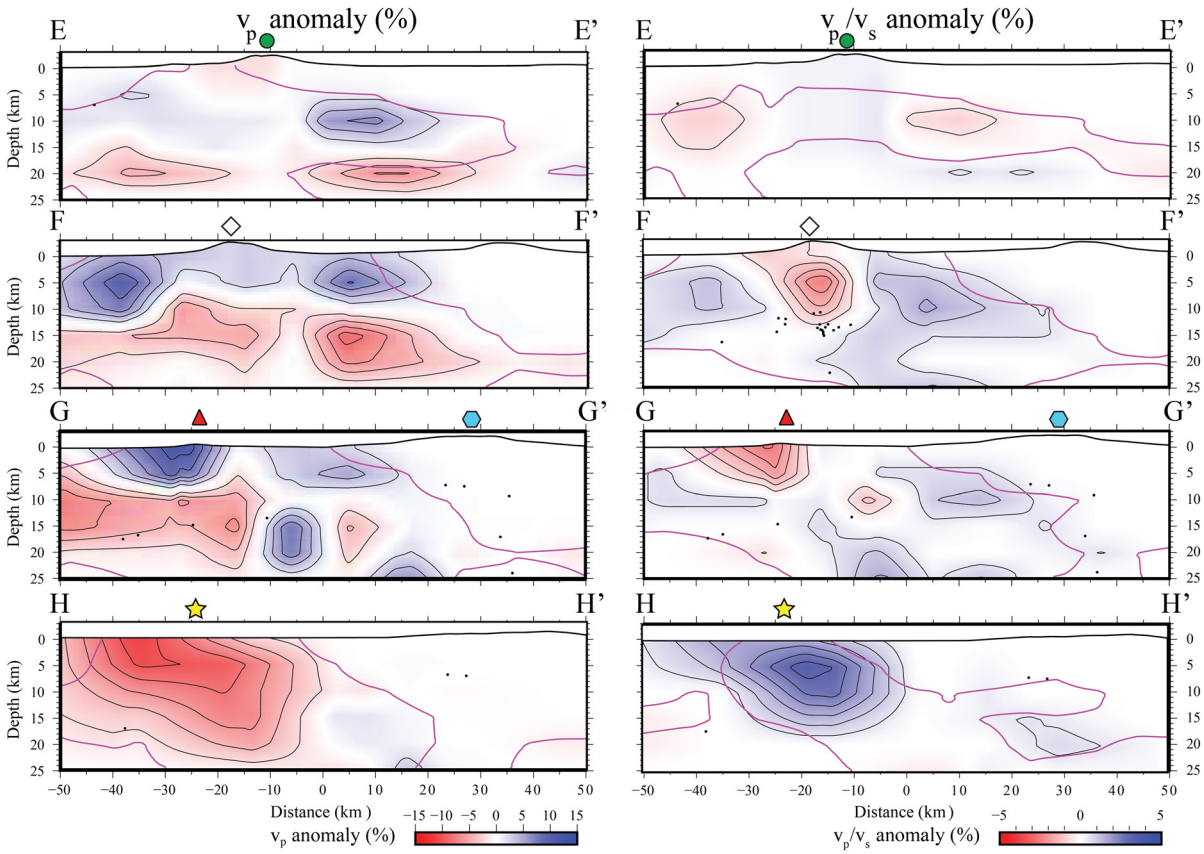

Fig. 8. Inverted V_p and V_p/V_s anomalies. The cross sections indicate that a major sub-horizontal discontinuity occurs at about 10 km depth separating regions characterised by positive and negative V_p anomalies. This is particularly visible in the V_p anomaly distributions of sections F-F' and G-G'.

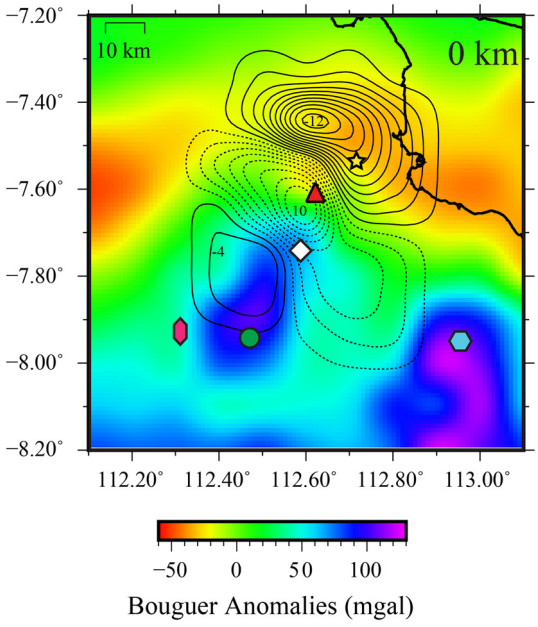

Fig. 9. Bouguer anomaly of the investigated region. The largest positive Bouguer anomalies occur beneath the active magmatic arc, broadly corresponding to the volcanic edifices. The Kendeng Basin and the region of the back-arc where Lusi crops out are characterised by negative Bouguer anomalies. Bouguer anomalies have been downloaded from the *International gravimetric bureau* http://bgi.omp.obs-mip.fr.

Clements et al., 2009; Novianto et al., 2020). Such structures do not crop out in the Kendeng basin to the north of the volcanic arc because alluvial deposits and rice fields do not allow geological surveying. However, the active seismic data collected for the exploration of hydrocarbon resources (Mazzini et al., 2007; Moscariello et al., 2018; Novianto et al., 2020) confirm a compressional and at times transpressional tectonics where lithologies are affected by frequent and widespread diapiric structures (Moscariello et al., 2018). The ongoing compressional regime, in addition to the sometimes locally elevated geothermal gradient of the region would help promoting the development of geological compartments at near-lithostatic pressure at depth. This, along with an ongoing hydrocarbon maturation process, would explain the frequent occurrence of diapiric structures in the Kendeng basin. Lusi is only the most recent piercement that reached the surface and it is proposed to occur where the Watukosek fault system would intersect a low angle fault along which fluids would flow from the volcanic arc into the back-arc basin.

7. Conclusions

Using the seismic catalogue recorded in the framework of LusiLab, and complementing it with data retrieved from additional stations from the Indonesian permanent network, we performed a local earthquake tomography of the East Java region. We obtained V_p and V_p/V_s anomaly distributions with respect to the initial velocity model. Such anomalies show sharp contrasts and regions marked by negative V_p and positive V_p/V_s perturbations. This allowed us to identify a region where large magmatic reservoirs are suggested to occur. The Kendeng basin, hosting the Lusi sediment hosted geothermal system features the largest negative V_p and positive V_p/V_s perturbations. The tomographic inversion shows that the Kendeng Basin is connected to the volcanic arc via a region characterised by negative V_p anomalies below about 10 km depth.

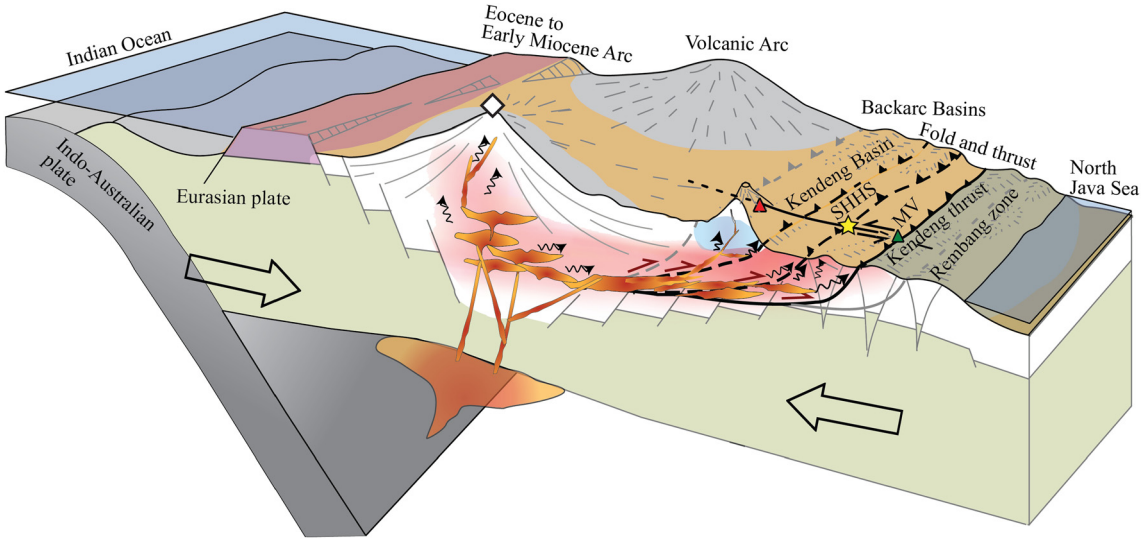

Fig. 10. Conceptual tectonic model suggesting the northwards migration of the volcanic arc. We propose that magmas from beneath the volcanic arc migrate northwards along low-angle thrust faults ultimately reaching the back-arc basins. Similarly, hydrothermal fluids would advect and promote vigorous convection in the permeable sedimentary units of the Kendeng Basin. Modified from Husein (2014).

The interpretation of the tomographic inversion allows us to propose a conceptual tectonic model that may help understanding the progression of the volcanic arc northwards. We suggest that the subduction-driven compressional regime promotes the formation of low-angle thrust faults departing from the volcanic arc. Along these regions, magmas and hydrothermal fluids would reach the back-arc flowing into the sedimentary basins and ultimately promoting the formation of sedimentary-hosted geothermal systems. The corollary is that Lusi is a natural occurrence and it may represent the inception of a newborn volcanic system.

CRediT authorship contribution statement

Pasquale De Gori, Luisa Valoroso, Paola Baccheschi and Riccardo Minetto revised and improved the seismic catalogue. Pasquale De Gori run the inversion. Adriano Mazzini and Matteo Lupi conceived the study and designed the seismic network. All authors contributed to the writing of the manuscript.

Declaration of competing interest

The authors declare that they have no known competing financial interests or personal relationships that could have appeared to influence the work reported in this paper.

Acknowledgements

The work was funded by the European Research Council under the European Union's Seventh Framework Program grant agreement 308126 (LusiLab project, PI A. Mazzini). We acknowledge the support from the Research Council of Norway through its Centers of Excellence funding scheme (project 223272) and the HOTMUD project (number 288299). Riccardo Minetto is funded by the URBASIS-EU project (H2020-MSCA-ITN-2018), grant 813137. We thank the Geophysical Instrument Pool Potsdam (GIPP) for providing the instruments for the SEED experiment in the framework of the LUSI LAB project. Matteo Lupi acknowledges the Swiss National Science Foundation for the funding scheme *Ambizione* (project PZ00P2 154815). The authors thank BPLS for their support during field operations and Karyono Karyono is thanked for the initial catalogue of the LusiLab temporary network. The data presented herein have been collected within the framework of the ERC project 308126 and the SNF project Ambizione (grant number PZ00P2_154815). We thank two anonymous reviewers for their constructive suggestions.

Appendix A. Supplementary material

Supplementary material related to this article can be found online at https://doi.org/10.1016/j.epsl.2021.117258.

References

Antunes, V., Planès, T., Zahradník, J., Obermann, A., Alvizuri, C., Carrier, A., Lupi, M., 2020. Seismotectonics and 1-D velocity model of the Greater Geneva Basin, France–Switzerland. Geophys. J. Int. 221, 2026–2047.

Clements, B., Hall, R., Smyth, H.R., Cottam, M.A., 2009. Thrusting of a volcanic arc: a new structural model for Java. Pet. Geosci. 15, 159–174.

Comino, J.Á.L., Heimann, S., Cesca, S., Milkereit, C., Dahm, T., Zang, A., 2017. Automated full waveform detection and location algorithm of acoustic emissions from hydraulic fracturing experiment. Proc. Eng. 191, 697–702.

Darman, H., 2000. An Outline of the Geology of Indonesia. Lereng Nusantara.

Eberhart-Phillips, D., Chadwick, M., 2002. Three-dimensional attenuation model of the shallow Hikurangi subduction zone in the Raukumara Peninsula, New Zealand. J. Geophys. Res., Solid Earth 107, ESE-3.

Eberhart-Phillips, D., Reyners, M., 1997. Continental subduction and three-dimensional crustal structure: the northern South island, New Zealand. J. Geophys. Res., Solid Earth 102, 11843–11861.

Elnashai, A.S., Kim, S.J., Yun, G.J., Sidarta, D., 2007. The Yogyakarta Earthquake of May 27, 2006. MAE Center CD Release 07-02.

Fallahi, M.J., Obermann, A., Lupi, M., Karyono, K., Mazzini, A., 2017. The plumbing system feeding the Lusi eruption revealed by ambient noise tomography. J. Geophys. Res., Solid Earth 122, 8200–8213.

Ferré, E.C., Galland, O., Montanari, D., Kalakay, T.J., 2012. Granite magma migration and emplacement along thrusts. Int. J. Earth Sci. 101, 1673–1688.

Galland, O., Cobbold, P.R., de Bremond d'Ars, J., Hallot, E., 2007. Rise and emplacement of magma during horizontal shortening of the brittle crust: insights from experimental modeling. J. Geophys. Res., Solid Earth 112.

Gunawan, E., Widiyantoro, S., 2019. Active tectonic deformation in Java, Indonesia inferred from a GPS-derived strain rate. J. Geodyn. https://doi.org/10.1016/j.jog.2019.01.004.

Haberland, C., Bohm, M., Asch, G., 2014. Accretionary nature of the crust of Central and East Java (Indonesia) revealed by local earthquake travel-time tomography. J. Asian Earth Sci. 96, 287–295.

Hall, R., Clements, B., Smyth, H.R., Cottam, M.A., 2007. A new interpretation of Java's structure.

Harris, A.J., Ripepe, M., 2007. Regional earthquake as a trigger for enhanced volcanic activity: evidence from MODIS thermal data. Geophys. Res. Lett. 34.

Husein, S., 2014. Trip Guide: Petroleum and Regional Geology Northeast Java Basin, Indonesia. The International Geology Course Programme.

Inguaggiato, S., Mazzini, A., Vita, F., Sciarra, A., 2018. The Arjuno-Welirang volcanic complex and the connected Lusi system: geochemical evidences. Mar. Pet. Geol. https://doi.org/10.1016/j.marpetgeo.2017.10.015.

Istadi, B.P., Pramono, G.H., Sumintadireja, P., Alam, S., 2009. Modeling study of growth and potential geohazard for LUSI mud volcano: East Java, Indonesia. Mar. Pet. Geol. 26, 1724–1739.

Karyono, K., Obermann, A., Nugraha, F., Sudradjat, A., Syafri, I., et al., 2020. The deep subsurface structure beneath Lusi and the adjacent volcanic chain inferred from local travel-time tomography. J. Volcanol. Geotherm. Res. 106919.

Koulakov, I., Bohm, M., Asch, G., Lühr, B.G., Manzanares, A., Brotopuspito, K., Fauzi, P., Purbawinata, M., Puspito, N., Ratdomopurbo, A., et al., 2007. P and S velocity structure of the crust and the upper mantle beneath central Java from local tomography inversion. J. Geophys. Res., Solid Earth 112.

Koulali, A., McClusky, S., Susilo, S., Leonard, Y., Cummins, P., Tregoning, P., Meilano, I., Efendi, J., Wijanarto, A.B., 2017. The kinematics of crustal deformation in Java from GPS observations: implications for fault slip partitioning. Earth Planet. Sci. Lett. 458, 69–79.

Lahr, J.C., 1999. HYPOELLIPSE: A Computer Program for Determining Local Earthquake Hypocentral Parameters, Magnitude, and First Motion Pattern. Citeseer.

Lupi, M., Mazzini, A., Sciarra, A., Collignon, M., Schmid, D.W., Husein, A., Romeo, G., Obermann, A., Karyono, K., 2018. Enhanced hydrothermal processes at the newborn Lusi eruptive system, Indonesia. J. Volcanol. Geotherm. Res. 366, 47–57.

Lupi, M., Saenger, E.H., Fuchs, F., Miller, S., 2013. Lusi mud eruption triggered by geometric focusing of seismic waves. Nat. Geosci. 6, 642–646.

Malvoisin, B., Mazzini, A., Miller, S.A., 2018. Deep hydrothermal activity driving the Lusi mud eruption. Earth Planet. Sci. Lett. 497, 42–49.

Manga, M., Brumm, M., Rudolph, M.L., 2009. Earthquake triggering of mud volcanoes. Mar. Pet. Geol. 26, 1785–1798.

Martha, A.A., Cummins, P., Saygin, E., Widiyantoro, S., et al., 2017. Imaging of upper crustal structure beneath East Java–Bali, Indonesia with ambient noise tomography. Geosci. Lett. 4, 1–12.

Maryanto, S., Wuryani, S.D., Nugraha, A.K., Prayogo, A., Kunrat, S.L., Basuki, A., 2017. Temporal changes of complete bougeuer anomalies at Bromo Volcano, East Java, Indonesia. Int. J. Appl. Eng. Res. 12, 10867–10873.

Mauri, G., Husein, A., Mazzini, A., Irawan, D., Sohrabi, R., Hadi, S., Prasetyo, H., Miller, S.A., 2018. Insights on the structure of Lusi mud edifice from land gravity data. Mar. Pet. Geol. 90, 104–115.

Mazzini, A., 2018. 10 years of Lusi eruption: lessons learned from multidisciplinary studies. (LUSI LAB).

Mazzini, A., Etiope, G., Svensen, H., 2012. A new hydrothermal scenario for the 2006 Lusi eruption, Indonesia. Insights from gas geochemistry. Earth Planet. Sci. Lett. 317–318, 305–318.

Mazzini, A., Hadi, S., Etiope, G., Inguaggiato, S., 2014. Tectonic control of piercement structures in Central Java, Indonesia. In: AGU Fall Meeting Abstracts, OS21B-1138.

Mazzini, A., Nermoen, A., Krotkiewski, M., Podladchikov, Y., Planke, S., Svensen, H., 2009. Strike-slip faulting as a trigger mechanism for overpressure release through piercement structures. Implications for the Lusi mud volcano, Indonesia. Mar. Pet. Geol. https://doi.org/10.1016/j.marpetgeo.2009.03.001.

Mazzini, A., Svensen, H., Akhmanov, G.G., Aloisi, G., Planke, S., Malthe-Sørenssen, A., Istadi, B., 2007. Triggering and dynamic evolution of the LUSI mud volcano, Indonesia. Earth Planet. Sci. Lett. 261 (3–4), 375–388.

Menand, T., Daniels, K., Benghiat, P., 2010. Dyke propagation and sill formation in a compressive tectonic environment. J. Geophys. Res., Solid Earth 115.

Menke, W., 1984. The resolving power of cross-borehole tomography. Geophys. Res. Lett. 11, 105–108.

Michelini, A., McEvilly, T., 1991. Seismological studies at parkfield. I. Simultaneous inversion for velocity structure and hypocenters using cubic b-splines parameterization. Bull. Seismol. Soc. Am. 81, 524–552.

Moscariello, A., Do Couto, D., Mondino, F., Booth, J., Lupi, M., Mazzini, A., 2018. Genesis and evolution of the Watukosek fault system in the Lusi area (East Java). Mar. Pet. Geol. 90, 125–137.

Nachrowi, T., Yohanes, M., Koesoemo, P., 2003. A geological trip to Cepu area for non-geoscientist personnel.

Novianto, A., Prasetyadi, C., Setiawan, T., et al., 2020. Structural model of Kendeng basin: a new concept of oil and gas exploration. Open J. Yangtze Oil Gas 5, 199–214.

Obermann, A., Karyono, K., Diehl, T., Lupi, M., Mazzini, A., 2018. Seismicity at Lusi and the adjacent volcanic complex, Java, Indonesia. Mar. Pet. Geol. 90, 149–156.

Prejean, S., Hill, D., Brodsky, E., Hough, S., Johnston, M., Malone, S., Oppenheimer, D., Pitt, A., Richards-Dinger, K., 2004. Remotely triggered seismicity on the United States west coast following the m w 7.9 Denali fault earthquake. Bull. Seismol. Soc. Am. 94, S348–S359.

Rosenberg, C.L., Berger, A., 2009. On the causes and modes of exhumation and lateral growth of the Alps. Tectonics 28.

Samankassou, E., Mazzini, A., Chiaradia, M., Spezzaferri, S., Moscariello, A., Do Couto, D., 2018. Origin and age of carbonate clasts from the Lusi eruption, Java, Indonesia. Mar. Pet. Geol. https://doi.org/10.1016/j.marpetgeo.2017.11.012.

Santoso, D., Wahyudi, E., Kadir, W., Alawiyah, S., Nugraha, A., Supendi, P., Parnadi, W., 2018. Gravity structure around Mt. Pandan, Madiun, East Java, Indonesia and its relationship to 2016 seismic activity. Open Geosci. 10, 882–888.

Sciarra, A., Mazzini, A., Inguaggiato, S., Vita, F., Lupi, M., Hadi, S., 2018. Radon and carbon gas anomalies along the Watukosek Fault System and Lusi mud eruption, Indonesia. Mar. Pet. Geol. https://doi.org/10.1016/j.marpetgeo.2017.09.031.

Setiadi, I., Setyanta, B., Nainggolan, T.B., Widodo, J., 2019. Delineation of sedimentary subbasin and subsurface interpretation East Java basin in the Madura strait and surrounding area based on gravity data analysis. Bull. Mar. Geol. 34.

Simo, T., Sekti, R.P., Hakiki, F., Sun, M., Myers, R.D., Fullmer, S., 2012. Reservoir characterization and simulation of an Oligocene-Miocene isolated carbonate platform: Banyu Urip field, East Java basin, Indonesia. In: Guidebook of Workshop of American Association of Petroleum Geologists.

Smyth, H., Hall, R., Hamilton, J., Kinny, P., 2005. East Java: Cenozoic basins, volcanoes and ancient basement.

Sribudiyani, N.M., Ryacudu, R., Kunto, T., Astono, P., Prasetya, I., Sapiie, B., Asikin, S., Harsolumakso, A.H., Yulianto, I., 2003. The collision of the East Java microplate and its implication for hydrocarbon occurrences in the East Java basin.

Subroto, E.A., Noeradi, D., Priyono, A., Wahono, H.E., Hermanto, E., Santoso, K., et al., 2007. The Paleogene basin within the Kendeng zone, Central Java Island, and implications to hydrocarbon prospectivity.

Tibaldi, A., 2005. Volcanism in compressional tectonic settings: is it possible? Geophys. Res. Lett. 32.

Toomey, D., Foulger, G., 1989. Tomographic inversion of local earthquake data from the Hengill-Grensdalur Central Volcano Complex, Iceland. J. Geophys. Res., Solid Earth 94, 17497–17510.

Wagner, D., Koulakov, I., Rabbel, W., Luehr, B.G., Wittwer, A., Kopp, H., Bohm, M., Asch, G., Scientists, M., 2007. Joint inversion of active and passive seismic data in Central Java. Geophys. J. Int. 170, 923–932.

Waltham, D., Hall, R., Smyth, H.R., Ebinger, C.J., 2008. Basin formation by volcanic arc loading. Spec. Pap., Geol. Soc. Am. 436, 11.

Widjajanti, N., Pratama, C., Parseno, Sunantyo, T.A., Heliani, L.S., Ma'ruf, B., Atunggal, D., Lestari, D., Ulinnuha, H., Pinasti, A., Ummi, R.F., 2020. Present-day crustal deformation revealed active tectonics in Yogyakarta, Indonesia inferred from GPS observations. Geod. Geodyn. https://doi.org/10.1016/j.geog.2020.02.001.

Wölbern, I., Rümpker, G., 2016. Crustal thickness beneath Central and East Java (Indonesia) inferred from P receiver functions. J. Asian Earth Sci. 115, 69–79.

Zaputlyaeva, A., Mazzini, A., Blumenberg, M., Scheeder, G., Kürschner, W.M., Kus, J., Jones, M.T., Frieling, J., 2020. Recent magmatism drives hydrocarbon generation in North-East Java, Indonesia. Sci. Rep. 10, 1–14.

Zaputlyaeva, A., Mazzini, A., Caracausi, A., Sciarra, A., 2019. Mantle-derived fluids in the East Java sedimentary basin, Indonesia. J. Geophys. Res., Solid Earth 124, 7962–7977.

Zhao, D., Hasegawa, A., Horiuchi, S., 1992. Tomographic imaging of P and S wave velocity structure beneath northeastern Japan. J. Geophys. Res., Solid Earth 97, 19909–19928.